Slow Magnetic Relaxation in a Mononuclear Eight-Coordinate Cobalt(II) Complex

Lei Chen[a], Jing Wang[a], Jin-Mei Wei,[b] Wolfgang Wernsdorfer,[c] Xue-Tai Chen,[a,*] Yi-Quan Zhang,[b,*] You Song,[a,*] and Zi-Ling Xue[d]

[a]*State Key Laboratory of Coordination Chemistry, Nanjing National Laboratory of Microstructures, School of Chemistry and Chemical Engineering, Nanjing University, Nanjing 210093, China;*

[b]*Jiangsu Key Laboratory for NSLSCS, School of Physical Science and Technology, Nanjing Normal University, Nanjing 210023, China;*

[c]*Institut Néel, CNRS, Nanoscience Department, BP 166, 380412 Grenoble Cedex 9, France;*

[d] *Department of Chemistry, University of Tennessee, Knoxville, Tennessee 37996, USA*

Supporting Information

Experimental Section

Materials and General Characterization:

All chemicals were purchased from commercial sources and used without further purification. The powder XRD patterns were recorded at room temperature on a BRUKER D8 ADVANCE X-ray diffractometer. Elemental analyses were performed on an Elementar Vario ELIII elemental analyzer.

Magnetic Measurements

Magnetic susceptibility data of **1** (m = 24.09 mg) were recorded with a Quantum Design SQUID VSM magnetometer at fields up to 7 T between 1.8 and 300 K. The temperature and frequency dependent alternate-current susceptibility measurements under different applied static magnetic fields were carried out using an oscillating ac field of 2.0 Oe and ac frequencies ranging from 1 to 1000 Hz. The magnetic susceptibilities data were corrected for the sample holder, as well as for diamagnetism of the constituent atoms (estimated using Pascal's constants).

Magnetization hysteresis loops on single crystal were measured by employing a micro-SQUID array in temperature range of 0.03-5.0 K and at field sweep rates varying in the range of 0.004-0.280 T s^{-1}.

High-Frequency and -Field EPR (HFEPR) were measured at the EMR Facility of the National High Magnetic Field Laboratory, Tallahassee, Florida.[S1,S2] The HFEPR frequency covered the range of 100 – 700 GHz, while the magnetic field varied from 0 to 25 T.

Synthesis of $[Co^{II}(12\text{-crown-}4)_2](I_3)_2(12\text{-crown-}4)$ (1)

Preparation of **1** was performed according the method of Meyer *et al.*[S3] To the solution of CoI_2 (1.0 mmol, 0.32 g) and 12-crown-4 (1.0 mmol, 0.16 ml) in 10 ml of acetonitrile was added the solution of I_2 (1.0 mmol, 0.254 g) in 5 ml of acetonitrile. The reaction mixture was stirred at 40 ^oC for 3 h, filtrated. The solution was left in a beaker until crystallization occurred. Black blocky crystals were isolated with a yield of 55 % based on Co. Anal. Calc. for $C_{24}H_{48}O_{12}I_6Co$: C, 21.36; H, 3.58. Found: C, 20.85; H, 3.57. The powder XRD measurement showed that the obtained sample is a monophase crystalline material (Figure. S1).

Computational Details

(Complete active space second-order perturbation theory) CASPT2 using MOLCAS 7.8 program package[S4] were performed on the complete structure of complex **1** to obtain the parameters *D* and *E*. For the first complete-active-space self-consistent field (CASSCF) calculation, the basis sets for all atoms are atomic natural orbitals from the MOLCAS ANO-RCC library: ANO-RCC-VTZP for magnetic center ion Co^{II}; VTZ for close O and N; VDZ for distant atoms. The calculations employed the second order Douglas-Kroll-Hess Hamiltonian, where scalar relativistic contractions were taken into account in the basis set. After that, the effect of the dynamical electronic correlation was applied using CASPT2. And then, the spin-orbit coupling was handled separately in the restricted active space state interaction (RASSI-SO) procedure. The active electrons in 10 active spaces include

all seven 3d electrons, and the mixed spin-free states are 50 (all from 10 quadruplets; all from 40 doublets).

To obtain the d-orbital energies, Orca 2.9.1 calculations[S5] were performed with the popular B3LYP hybrid functional proposed by Becke[S6,S7] and Lee et al.[S8] Triple-ζ with one polarization function TZVP[S9] basis set was used for all atoms. The scalar relativistic treatment (ZORA) was used in all calculations. The large integration grid (grid = 6) was applied to Co(II) for ZORA calculations. Tight convergence criteria were selected to ensure that the results were well converged with respect to technical parameters.

In order to study the effect of the structural distortions due to the change of the angles φ and α in the electronic structures on the magnetic anisotropy, three states are assumed for the calculations. State **c** is assumed for ideal square antiprism ($\varphi = 45^{o}$, $\alpha = 54.74^{o}$), which will be converted to two intermediate states (state **a**: $\varphi = 39.07^{o}$, $\alpha = 54.74^{o}$; state **b**: $\varphi = 45^{o}$, $\alpha = 55.69(5)\text{-}56.55(5)^{o}$) via changing the angles φ and α, respectively. CASPT2 calculations were also performed on the assumed states of **a**-**c**. The calculated electronic configuration and d-orbital energy level diagrams for complex **1** and states **a**-**c** are shown in the following Figure S6 and Scheme S1. The calculated energy levels are listed in Table S2.

Additional Magnetic Susceptibility Fitted Using ANISOFIT 2.0[S10]

To determine the sign and value of zero-field splitting parameters, fits were attempted on the M versus H/T data using ANISOFIT 2.0[S10] where the initial *D* and *E*

values were varied for each the fitting process. Five final results were obtained through setting the approximate twenty sets of the initial values, as shown in Table S1. Two output results were obtained for setting the positive initial D values (No. 1 and 2), while two results were obtained for setting the negative initial D values (No. 3 and 4). The data of No. 1 is excluded due to the large agreement factor f. The results of No. 2 are not reasonable because they do not meet $|3E| \leq |D|$. The best fit (No. 3 and No. 4) suggests that the negative sign for the D value. Refer to the values of ZFS parameters obtained from the $\chi_M T$ data fit by the PHI program, we choose the value of No. 4 as the final result.

Table S1. Several optimized final results using ANISOFIT 2.0.

	$D > 0$					$D < 0$			
	D (cm^{-1})	$\|E\|$ (cm^{-1})	g	f		D (cm^{-1})	$\|E\|$ (cm^{-1})	g	f
No.1	26.32	25.25	2.45	0.022	No.3	-37.83	0.057	2.55	0.0012
No.2	320.8	0.015	2.44	0.26	No.4	-37.97	0.75	2.55	0.0012

Table S2. The calculated d-orbital energy levels (10^3 cm^{-1}) for **1** and states **a-c**

d-oribital	**a**	**b**	**c**	**d** (complex **1**)
d_{xy}	0	2.811	2.546	0
d_{xz}	1.517	2.425	1.887	2.721
d_{yz}	1.776	2.836	2.098	2.708
d_{z^2}	0.193	0.075	0.233	0.160
$d_{x^2-y^2}$	2.140	0	0	2.043

Table S3. Relaxation times τ (s) and α values for **1**

T (K)	τ (s)	α
1.8	0.00058	0.32
2.0	0.00041	0.30
2.2	0.00028	0.28
2.4	0.00022	0.24
2.6	0.00016	0.16
2.8	0.00012	0.16
3.0	0.00009	0.10
3.2	0.00007	0.07
3.4	0.00005	0.04
3.6	0.00004	0.04
3.8	0.00003	0.04
4.0	0.00002	0.06
4.2	0.00001	0.03
4.4	0.00001	0.03
4.6	7.26E-6	0.05
4.8	5.04E-6	0.06

Scheme S1. Structural transformation from the ideal square antiprism to complex **1** and the calculated values of the ZFS parameters and g-factor for all states.

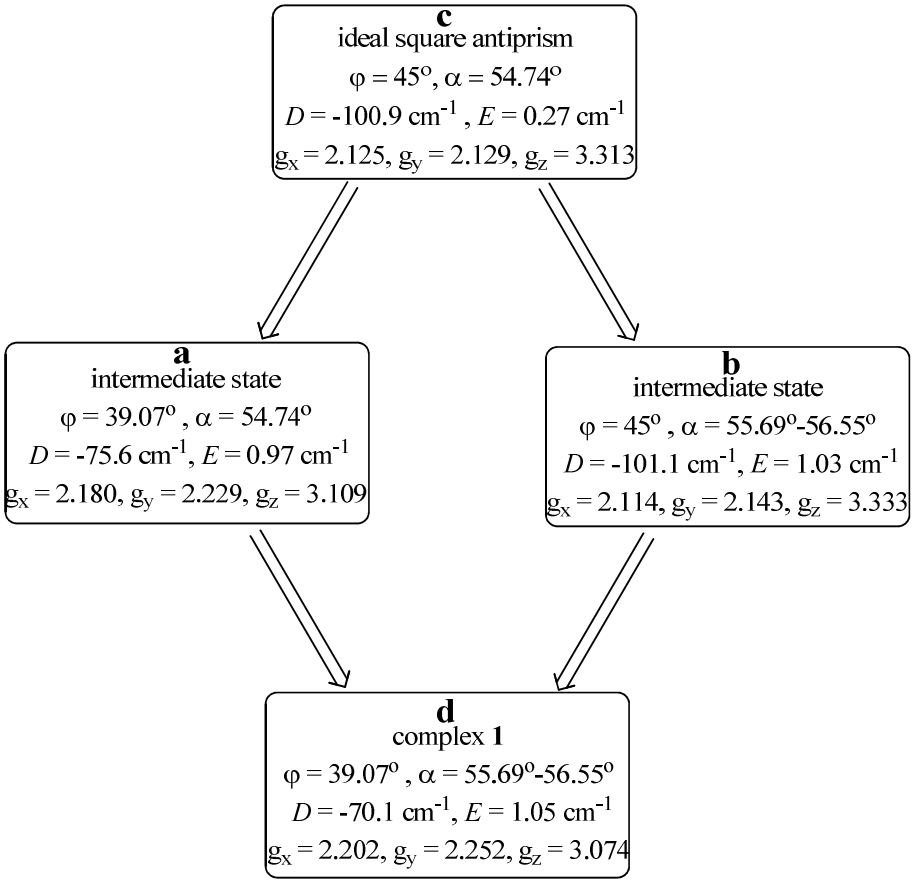

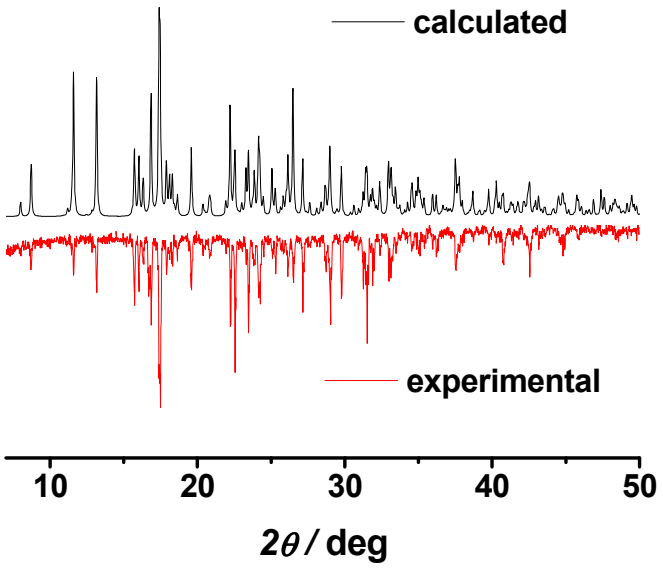

Figure S1. Powder XRD pattern for compound **1.**

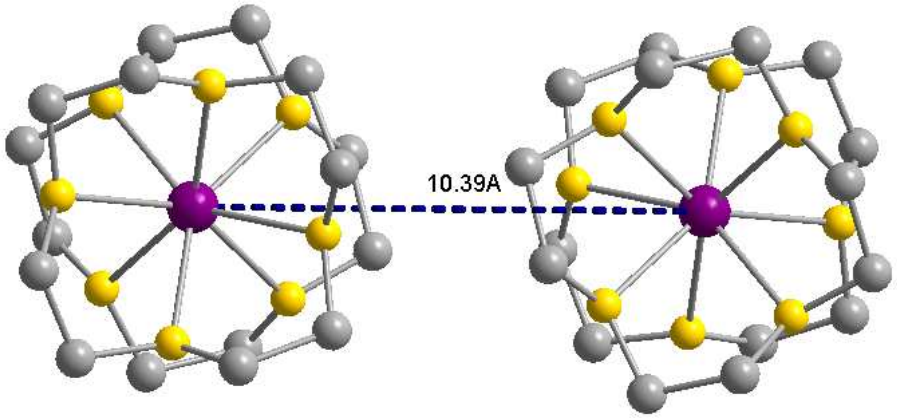

Figure S2. The shortest distance of Co(II) ions between neighbor clusters are 10.39 Å.

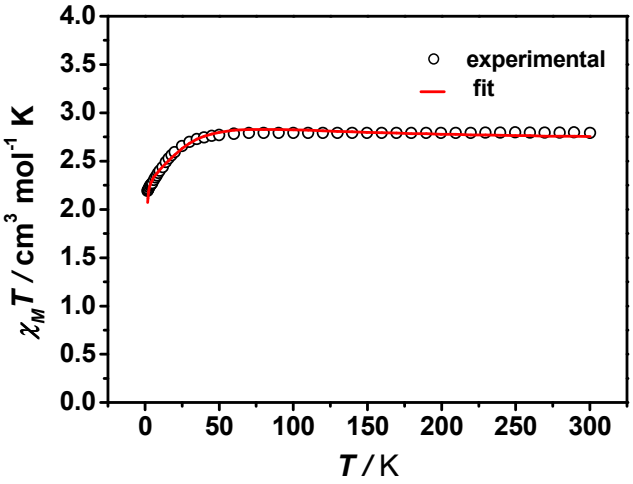

Figure S3. Variable temperature dc susceptibility data under 2000 Oe applied dc field of a pure ploy crystalline sample of **1**. Solid lines indicate the best fits with the PHI program[S11] yielding the spin-Hamiltonian parameters D = –37.6 cm^{-1}, E = 0.1 cm^{-1}, $g_{x,y}$ = 2.14, and g_z = 2.83, as discussed in the main text.

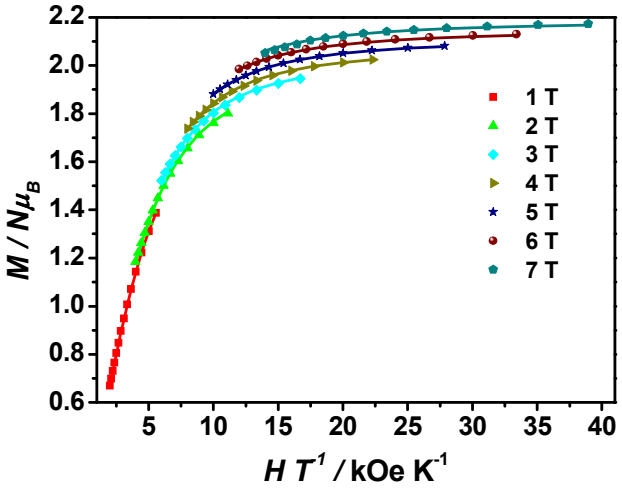

Figure S4. Variable-temperature, variable-field dc magnetization data collected on a polycrystalline sample of **1**. Fields of 1 to 7 T were used at temperatures from 1.8 to 5 K. Solid lines indicate the best fits with the program ANISOFIT 2.0[S10] yielding the spin-Hamiltonian parameters g = 2.55, D = – 38.0 cm^{-1} and E = – 0.75 cm^{-1} (f = 0.0012), as discussed in the main text.

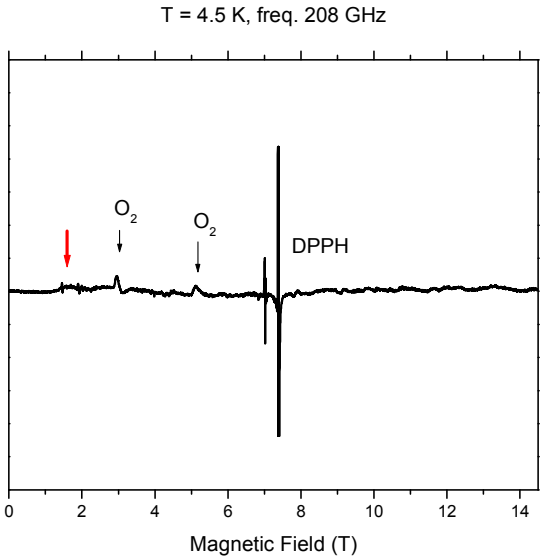

Figure S5. An 208 GHz EPR spectrum of **1** at 4.5 K. The red arrow points at the only resonance that could be attributed to high-spin Co(II).

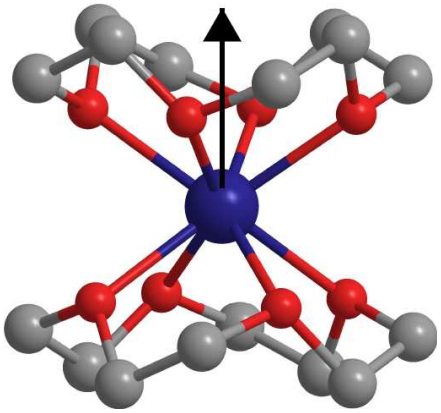

Figure S6. Orientation of the local main magnetic axis of the ground Kramers doublet on Co^{II} ion in **1**.

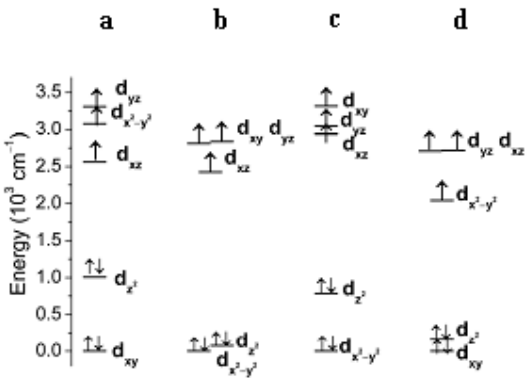

Figure S7. Electronic configuration and d-orbital energy level diagram for the molecule from DFT calculation. Labels **a**, **b**, **c**, and **d** correspond to the states indicated in Scheme 1.

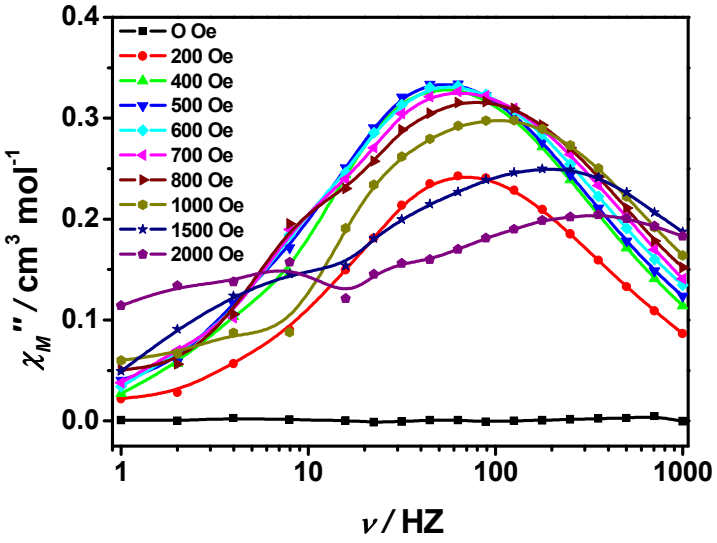

Figure S8. Frequency dependence of the out-of-phase (χ_M'') ac susceptibility at 2 K under the applied static field from 0 to 2000 Oe. The solid lines are for eye guide.

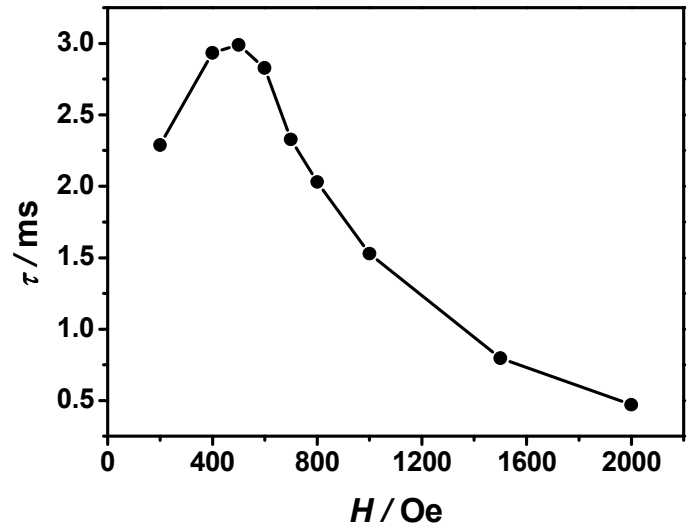

Figure S9. Field dependence of the magnetic relaxation time, τ, of a polycrystalline sample of **1** at 2 K.

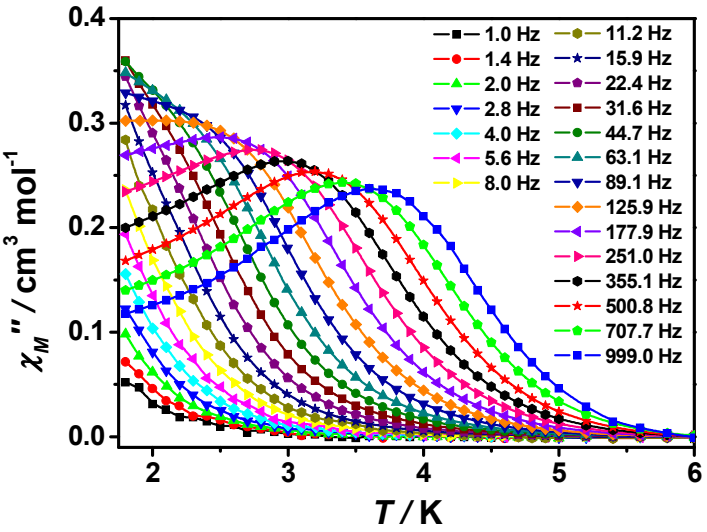

Figure S10. Temperature dependence of out-of-phase ac susceptibility at different ac frequency under a 500 Oe dc field for **1**. The solid lines are for eye guide.

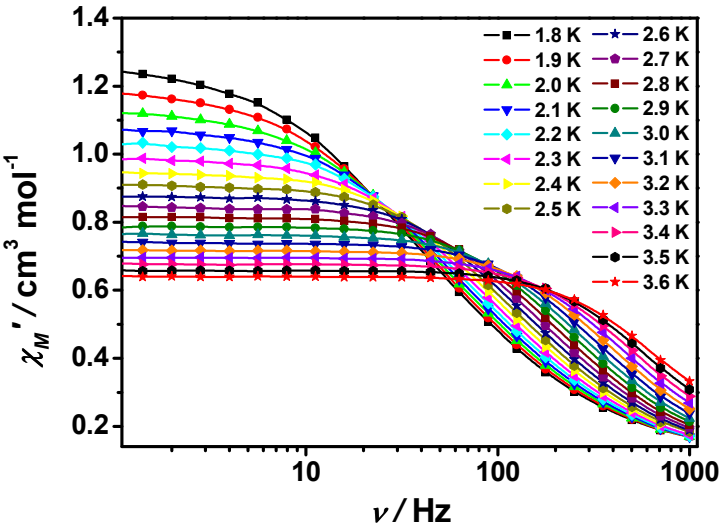

Figure S11. Frequency dependence of the in-phase ac susceptibility from 1.8 to 3.6 K under 500 Oe dc field for **1**. The solid lines are for eye guide.

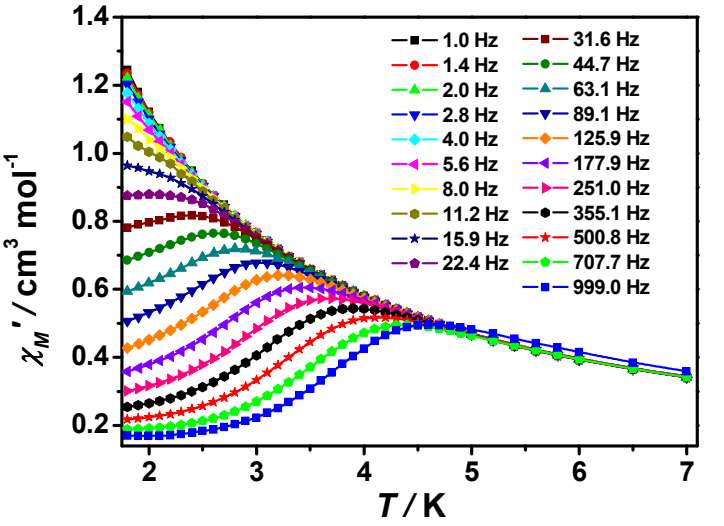

Figure S12. Temperature dependence of in-phase ac susceptibility at different ac frequency under a 500 Oe dc field for **1**. The solid lines are for eye guide.

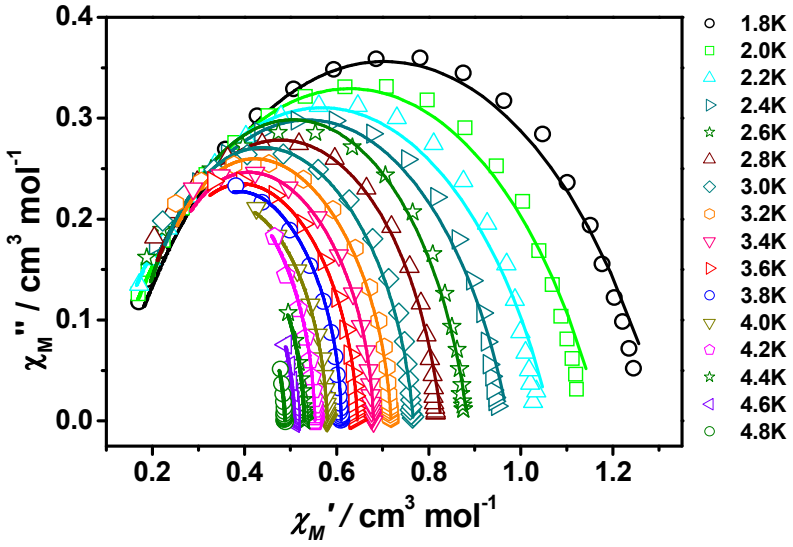

Figure S13. Cole-Cole plot obtained from the ac susceptibility data under 500 Oe dc field in the temperature range of 1.8- 4.8 K for **1**. Solid lines represent best fits to a generalized Debye model.

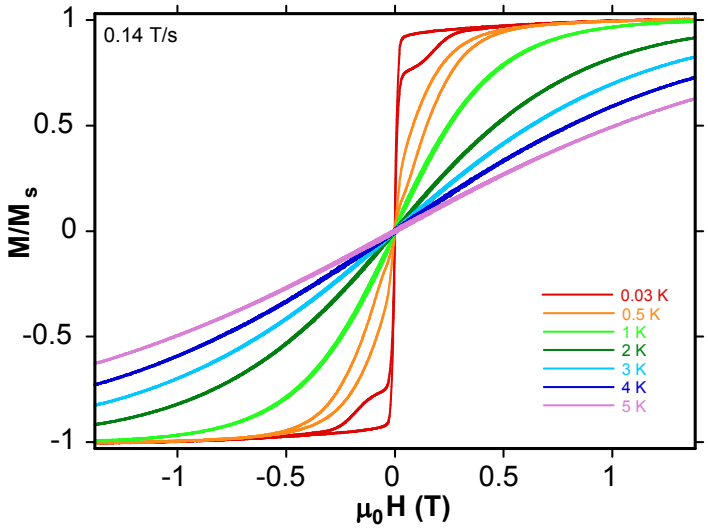

Figure S14. Field dependence of the normalized magnetization of **1** in the temperature rang 0.03-5 K at the field-sweep rate of 0.14 T s^{-1}.

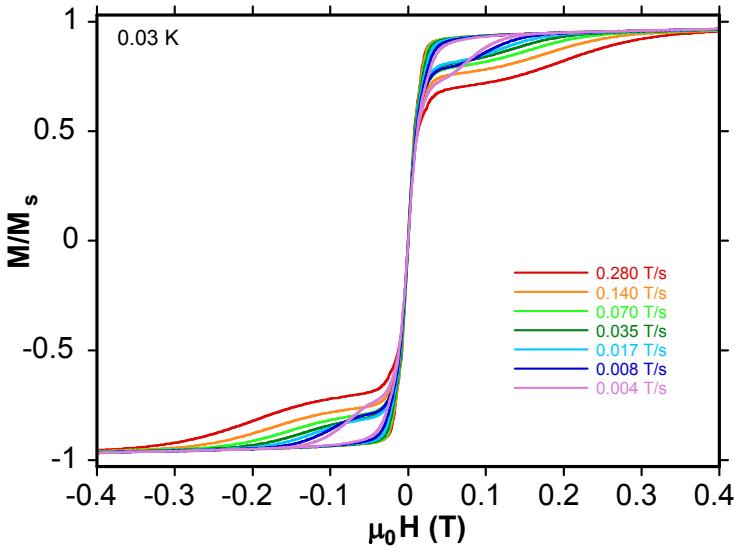

Figure S15. Field dependence of the normalized magnetization of **1** at 0.03 K with field sweep rates varying in the range of 0.004-0.280 T s^{-1}.

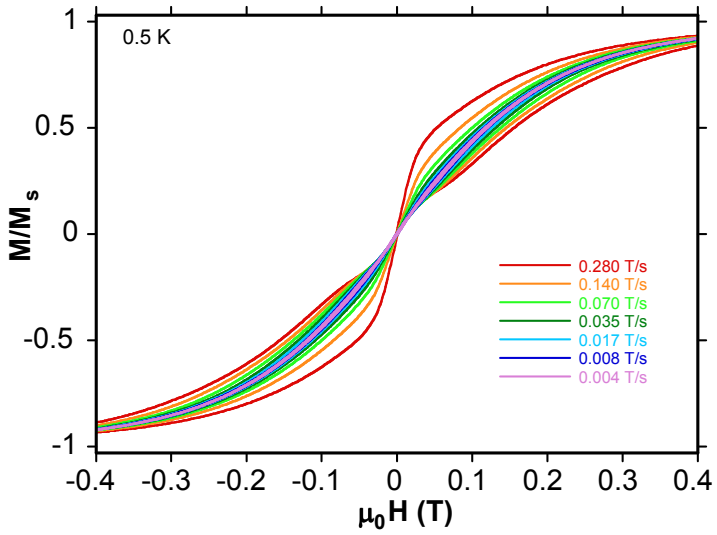

Figure S16. Field dependence of the normalized magnetization of **1** at 0.5 K with field sweep rates varying in the range of 0.004-0.280 T s^{-1}.

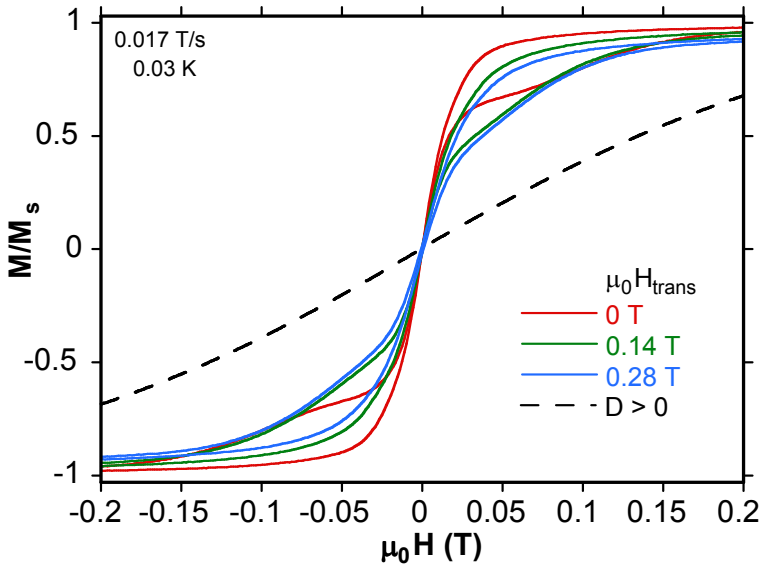

Figure S17. The normalized magnetization of **1** at 0.03 K at field-sweep rate 0.017 T s^{-1} under various external transverse field. The figure above shows hysteresis loops where the field was ligned with the easy axis of magnetization.[S12] If *D* were positive, the loops would smear out like indicated by the dashed curve.

Additional References

S1 Zvyagin, S. A.; Krzystek, J.; van Loosdrecht, P. H. M.; Dhalenne, G.; Revcolevschi, A., *Physica B* **2004**, *346-347*, 1.

S2 Hassan, A. K.; Pardi, L. A.; Krzystek, J.; Sienkiewicz, A.; Goy, P.; Rohrer, M.; Brunel, L. C. *J. Magn. Reson*. **2000**, *142*, 300.

S3 Fiolka, C.; Pantenburg, I.; Meyer, G. *Cryst. Growth Des.* **2011**, *11*, 5159.

S4 Karlstrom, G.; Lindh, R.; Malmqvist, P. A.; Roos, B. O.; Ryde, U.; Veryazov, V.; Widmark, P. O.; Cossi, M.; Schimmelpfennig, B.; Neograd y, P.; Seijo, L. *Comput*. *Mater*. *Sci*. **2003**, *28*, 222.

S5 Neese, F. ORCA-*an ab initio, density functional and semiempirical program package*, version 2.9.1; Max-Planck institute for bioinorganic chemistry: Mülheim an der Ruhr, Germany, 2012.

S6 Becke, A. D. *J. Chem. Phys*. **1993**, *98*, 5648.

S7 Becke, A. D. *Phys. Rev. A*. **1988**, *38*, 3098.

S8 Lee, C.; Yang, W.; Parr, R. G. *Phys. Rev. B*. **1988**, *37*, 785.

S9 (a) Schafer, A.; Horn, H.; Ahlrichs, R. *J. Chem. Phys*. **1992**, *97*, 2571. (b) Schafer, A.;Huber, C.; Ahlrichs, R. *J. Chem. Phys*. **1994**, *100*, 5829.

S10 Shores, M. P.; Sokol, J. J.; Long, J. R. *J. Am. Chem. Soc*. **2002**, *124*, 2279.

S11 Chilton, N. F.; Anderson, R. P.; Turner, L. D.; Soncini, A.; Murray, K. S. *J. Comput. Chem*. **2013**, *34*, 1164.

S12 Wernsdorfer, W.; Chakov, N. E.; Christou, G. *Phys. Rev. B* **2004**, *70*, 132413.